

Regulation by Oligomerization in a Mycobacterial Folate Biosynthetic Enzyme

Celia W. Goulding¹, Marcin I. Apostol², Michael R. Sawaya¹
Martin Phillips², Angineh Parseghian² and David Eisenberg^{1,2*}

¹Molecular Biology Institute
UCLA-DOE Institute of
Genomics and Proteomics
P.O. Box 951570, Los Angeles
CA 90095-1570, USA

²Department of Chemistry and
Biochemistry, UCLA, LA
CA 90095-1570, USA

Folate derivatives are essential cofactors in the biosynthesis of purines, pyrimidines and amino acids across all forms of life. Mammals uptake folate from their diets, whereas most bacteria must synthesize folate *de novo*. Therefore, the enzymes in the folate biosynthetic pathway are attractive drug targets against bacterial pathogens such as *Mycobacterium tuberculosis*, the cause of the world's most deadly infectious disease, tuberculosis (TB). *M. tuberculosis* 7,8-dihydroneopterin aldolase (*Mtb* FolB, DHNA) is the second enzyme in the folate biosynthetic pathway, which catalyzes the conversion of 7,8-dihydroneopterin to 6-hydroxymethyl-7,8-dihydropterin and glycoaldehyde. The 1.6 Å X-ray crystal structure of *Mtb* FolB complexed with its product, 6-hydroxymethyl-7,8-dihydropterin, reveals an octameric assembly similar to that seen in crystal structures of other FolB homologs. However, the 2.5 Å crystal structure of unliganded *Mtb* FolB reveals a novel tetrameric oligomerization state, with only partially formed active sites. A substrate induced conformational change appears to be necessary to convert the inactive tetramer to the active octamer. Ultracentrifugation confirmed that in solution unliganded *Mtb* FolB is mainly tetrameric and upon addition of substrate FolB is predominantly octameric. Kinetic analysis of substrate binding gives a Hill coefficient of 2.0, indicating positive cooperativity. We hypothesize that *Mtb* FolB displays cooperativity in substrate binding to regulate the cellular concentration of 7,8-dihydroneopterin, so that it may function not only as a precursor to folate but also as an antioxidant for the survival of *M. tuberculosis* against host defenses.

© 2005 Elsevier Ltd. All rights reserved.

Keywords: tetrahydrofolate biosynthesis; *Mycobacterium tuberculosis*; X-ray crystallography; allosteric regulation; 7,8-dihydroneopterin aldolase

*Corresponding author

Introduction

Tuberculosis (TB) is the most deadly infectious disease in the world and is caused by the bacterial pathogen, *Mycobacterium tuberculosis*. In recent decades, the increase in TB incidence has been so great that the World Health Organization (WHO) declared TB a global public health emergency.¹ As part of the response to this challenge, the TB structural genomics consortium† seeks to determine *M. tuberculosis* protein structures as potential

drug targets and also to gain a better understanding of mycobacterial pathogenesis.² One group of potential protein targets are those involved in essential biosynthetic pathways. Here we focus on one such pathway, the biosynthesis of folate.

Folate and its derivatives are essential cofactors in the biosynthesis of purines, pyrimidines and amino acids, and therefore folate is essential across all three domains of life.³ Mammalian cells are able to utilize pre-formed folate after uptake by a carrier-mediated active transporter system, whereas microbes, such as *M. tuberculosis*, lack this transporter system and must synthesize folate *de novo* from guanosine triphosphate.^{4,5} Hence, enzymes involved in the biosynthesis of folate are essential in bacteria and therefore make excellent drug targets against TB.³ 7,8-Dihydroneopterin aldolase (DHNA/FolB) is involved in the second step of

Abbreviations used: *Mtb*, *Mycobacterium tuberculosis*; TB, tuberculosis; FolB, DHNA, 7,8-dihydroneopterin aldolase.

E-mail address of the corresponding author:
david@mbi.ucla.edu

† <http://www.doe-mpi.ucla.edu/TB>

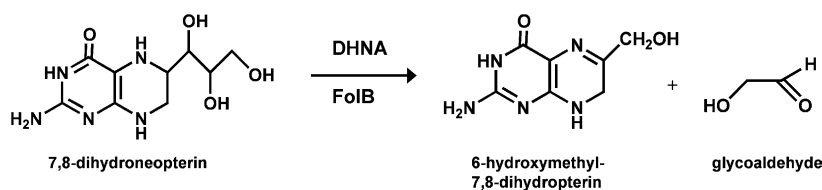


Figure 1. The reaction for the second step in folate biosynthesis, 7,8-dihydroneopterin aldolase (FolB or DHNA), which converts 7,8-dihydroneopterin to 6-hydroxymethyl-7,8-dihydropterin and glycoaldehyde.

folate biosynthesis, catalyzing the conversion of 7,8-dihydroneopterin to 6-hydroxymethyl-7,8-dihydropterin and glycoaldehyde⁶ (Figure 1). FolB is conserved across bacterial species and no mammalian FolB homologs have been identified thus far, making FolB an attractive potential drug target against *M. tuberculosis*. Our study describes two three-dimensional crystal structures of *M. tuberculosis* FolB (*Mtb* FolB), and we discuss their structural and biological implications.

Results

The structure of the octameric $P2_1$ form of *Mtb* FolB

Improving the resolution of the structure

After obtaining poorly diffracting crystals (4.8 Å resolution) of *Mtb* FolB-His₆-tag, the C-terminal His₆-tag was cleaved with thrombin which improved diffraction dramatically. Mass spectrometry results by MALDI/TOF of the thrombin cleaved *Mtb* FolB gave a mass of 13,647(±10) Da. This mass indicates that the protein had been cleaved between residues Arg120 and Gly121, a natural cleavage site found in *Mtb* FolB, resulting in the loss of the final 13 residues of *Mtb* FolB (Figure 2(a)). The crystals obtained after removal of the His₆-tag diffracted to higher resolution (2.0 Å) in space group $P2_1$ with eight monomers per asymmetric unit. The three-dimensional crystal structure was determined by molecular replacement using the octameric structure of *Staphylococcus aureus* FolB as a model (PDB-ID: 1DHN).⁷ The structure of the *Mtb* FolB octamer consists of two tetrameric rings which join to form a cylindrical structure around a central pore (Figure 2(b)), as seen for the *S. aureus* FolB structure.

Refinement of the model revealed electron density corresponding to a molecule bound in the active site. Models of both the FolB substrate, 7,8-dihydroneopterin, and the product, 6-hydroxymethyl-7,8-dihydropterin, were tested to fit residual electron density in the active site. The product produced the best fit. There is one product molecule bound per active site which is situated at the interface of two subunits, as a result there are eight equivalent active sites per octamer (Figure 2(b)). The resolution could be extended to 1.6 Å by soaking 7,8-dihydroneopterin into the $P2_1$ crystals. The refined 1.6 Å structure of *Mtb* FolB revealed the bound product 6-hydroxymethyl-7,8-dihydropterin.

The model displays good geometry with a final R_{work} of 16.5 and R_{free} of 25.8 (Table 1).

Refinement of the tetrameric $I4$ form of *Mtb* FolB

Mtb FolB also crystallized in space group $I4$ with one monomer per asymmetric unit. This *Mtb* FolB crystal form was solved by using the monomer from the $P2_1$ *Mtb* FolB structure as a probe for molecular replacement. The refinement was initially carried out with all the loops deleted from the model (Figure 2(a)). Most of the residues in the loop regions were rebuilt into electron density except for loop L1 (residues 15–25) as there was no observable electron density for residues Arg15 to Ala25. The refined $I4$ *Mtb* FolB model (2.5 Å) gave final R_{work} and R_{free} values of 17.9% and 23.4%, respectively, as stated in Table 1. This model has R -factors which may be considered high for this resolution data. There are two possible explanations for the discrepancy. The Wilson B factor and average B factor for the model are 51.7 Å² and 37.2 Å², indicating the presence of thermal or static disorder. Difficulty in modeling this disorder could account for the high R -factor. In addition there are local regions in the model which are disordered, the loop L1 (residues 15–25) which accounts for 10% of the residues of *Mtb* FolB and the side-chains of four other residues (Arg70, Lys71, Leu72 and Lys99) which were modeled as alanine residues.

Differences between *Mtb* FolB in the $P2_1$ and $I4$ crystal structures

Overall differences in oligomeric states observed in the $P2_1$ and $I4$ crystal forms

The overall tetrameric structure is conserved between the $P2_1$ and $I4$ *Mtb* FolB structures but in $P2_1$, the tetramers further associate into an octamer. Within space group $P2_1$, two tetramers of *Mtb* FolB related by a local 2-fold rotated symmetry axis, pack together as an octamer, i.e. “head-to-head” (Figure 3(a)). In contrast, the tetramers within space group $I4$ do not pack “head-to-head” and the octameric assembly is not present (Figure 3(b)). Hence, the two structures of *Mtb* FolB show an octamer in space group $P2_1$ and a tetramer in space group $I4$. Strands β 1– β 4, and helices α 3 and α 4 are conserved in both crystal structures. However, there are variations in the ligand binding and the loop regions L1, L2 and L4 between the two monomeric structures (Figure 4(a) and (b)).

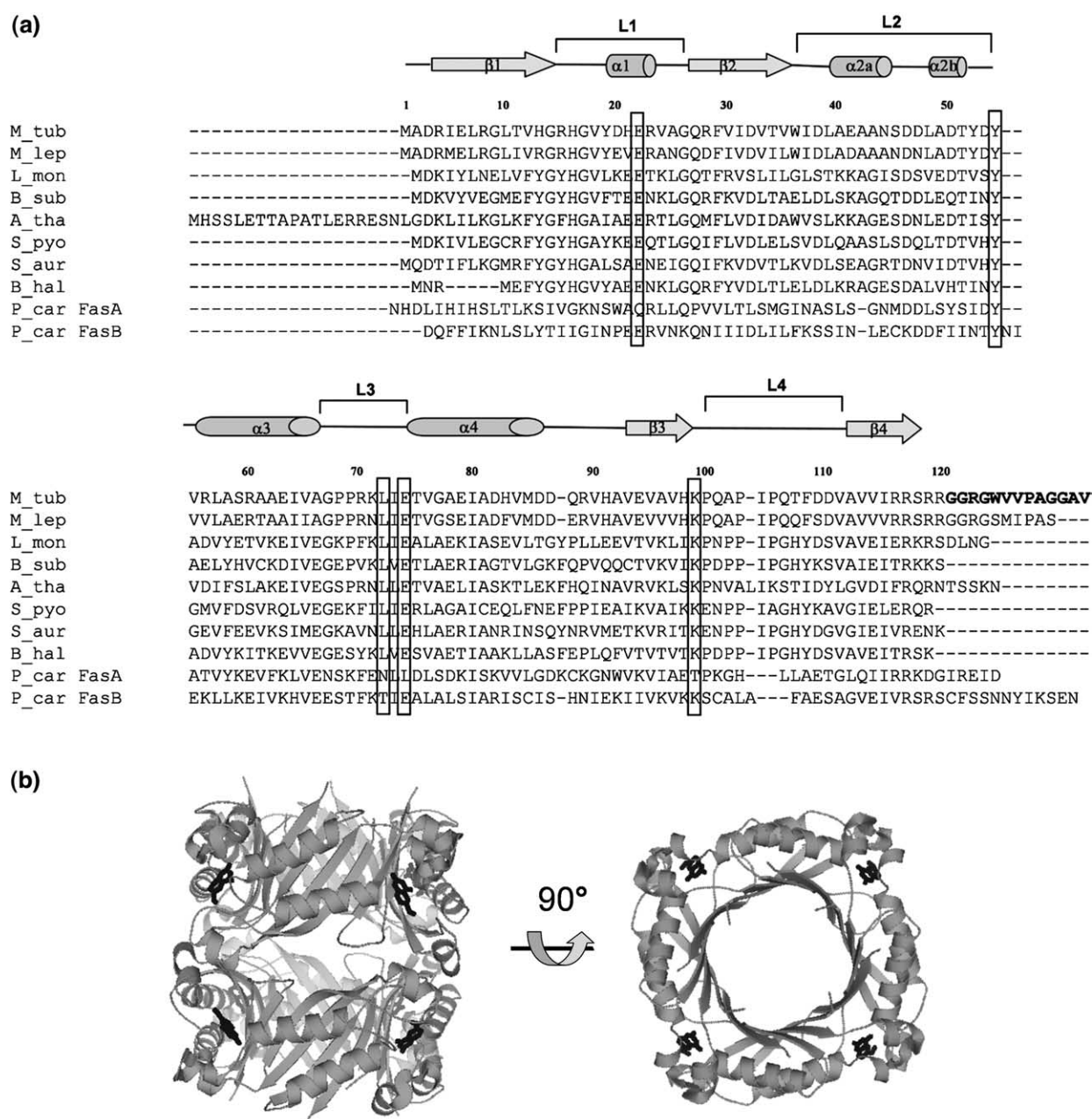


Figure 2. The sequence alignment of FolB homologs and three-dimensional structure of octameric *Mtb* FolB of the P₂₁. (a) The sequence alignment of FolB homologs. The top line depicts the *Mtb* FolB secondary structure elements which are aligned with the amino acid sequence. The arrows depict the β -strands, the cylinders depict the α -helices and 3_{10} -helix; the α -helices and β -strands are numbered. The first amino acid sequence is that of *Mtb* FolB and the bold grey letters show the C termini 13 amino acid residues lost after thrombin cleavage. The numbers directly above the amino acid sequences correspond to the residue numbers of *Mtb* FolB. The highly conserved residues which are mentioned in the text are highlighted with boxes, Glu22, Tyr54, Leu72, Glu74 and Lys99. The loops regions are designated L1, L2, L3 and L4. The abbreviation of the species names are as follows: M_tub, *M. tuberculosis*; M_lep, *Mycobacterium leprea*; L_mon, *Listeria monocytogenes*; E_coli, *Escherichia coli*; B_hal, *Bacillus haloduran*; P_aeru, *Pseudomonas aeruginosa*; A_thal, *Arabidopsis thaliana*; B_sub, *Bacillus subtilis*; S_pyo, *Streptococcus pyogenes*; P_car, *Pneumocystis carinii*. The sequence alignment was made with CLUSTALW and BoxShade. (b) Three-dimensional structure of octameric *Mtb* FolB of the P₂₁. The octamer is formed by a dimer of tetramers. Between each monomer is a stick model of a single product molecule of *Mtb* FolB, 6-hydroxymethyl-7,8-dihydropterin. A 90° rotation of the octameric *Mtb* FolB illustrates the top of the tetramer, where one can see 6-hydroxymethyl-7,8-dihydropterin more clearly. These Figures were created in PYMOL.

Differences in ligand binding

One of the most interesting differences between the two structures is the lack of an active-site ligand

in the tetrameric structure, whereas the octameric structure shows product bound (Figure 4(c)). The electron density within the active site of the octameric structure shows that the product fits

Table 1. X-ray diffraction data collection and atomic refinement for *Mtb* 7,8-dihydroneopterin aldolase in space groups $P2_1$ and $I4$

	Space group	
	$P2_1$	$I4$
No. of monomers per asymmetric unit	8	1
Unit cell dimensions (Å)	78.69×85.14×74.67	73.0×73.0×42.8
pH of crystallization condition	4.6	7.5
<i>Data set</i>		
Wavelength (Å)	0.9786	0.9786
Resolution range (Å)	100–1.60	100–2.5
Unique reflections (total)	118,216 (111,905)	3990 (37,961)
Completeness (%) ^a	99.2 (93.9)	99.0 (100.0)
R_{merge} ^{a,b}	6.9 (50.0)	7.8 (37.1)
I/σ^a	17.6 (1.9)	31.3 (7.6)
<i>Model refinement</i>		
Resolution range (Å)	20–1.6	20–2.5
No. of reflections (working/free)	91,628/4817	3532/404
No. of protein atoms	7406	819
No. of water molecules	470	22
No. of product atoms	112	0
No. of acetate atoms	0	8
$R_{\text{work}}/R_{\text{free}}^c$ (%)	16.5/25.8	17.9/23.4
<i>rms deviations</i>		
Bond lengths (Å)	0.019	0.018
Bond angles (deg.)	2.2	2.3
B-values average (Å ²)	24.0	37.8
<i>Ramachandran plot</i>		
Most favorable region (%)	96.0	83.3
Additional allowed region (%)	4.0	16.7
Disallowed region	0	1 residue, Pro69
Missing residues	0	15–25
PDB ID code	1NBU	1Z9W

Crystals in space group $P2_1$ were soaked overnight with 5 mM 7,8-dihydroneopterin.

^a Statistics for the highest resolution shell are given in (parentheses).

^b $R_{\text{merge}} = \sum |I - \langle I \rangle| / \sum I$.

^c $R_{\text{work}} = \sum |F_{\text{obs}} - F_{\text{calcd}}| / \sum F_{\text{obs}}$ was computed identically except where all reflections belong to a test set of randomly selected data.

extremely well (Figure 4(c) and (e)). In contrast, the tetrameric structure has no observable electron density for product but instead shows electron density corresponding to residues of the 3_{10} -helix $\alpha 2b$ within the vicinity of the active site (Figure 4(d) and (f)), which blocks substrate or product binding. This suggests that the apo-tetrameric state is the inactive form of *Mtb* FolB and the octameric state with product bound is the active form of the enzyme.

Differences in loop conformations

Another difference between the two structures is within the loop regions. Loop L1 (residues 15–25) which contains helix $\alpha 1$ and connects strand $\beta 1$ to strand $\beta 2$ in the octameric structure (Figure 4(a)) is a flexible, disordered loop in the apo-tetrameric structure, suggested by the lack of observable electron density (Figure 4(b)). Within the loop L2 region, the ordered helix $\alpha 2a$ in the octamer loses its secondary structure to form an extended loop in the apo-tetramer while the 3_{10} -helix $\alpha 2b$ has shifted its position into the vicinity of the active site (Figure 4(a) and (b)). Also, loop L4 is rotated approximately 80° from apo-tetrameric state to octameric state. These subtle conformation changes in the loop regions L1, L2 and L4 must occur in the

apo-tetrameric state upon substrate binding, in addition the conformation changes in loops L1 and L4 allow for octamer formation (Figure 5).

Various oligomeric states of *Mtb* FolB in solution

To determine whether the difference in the crystal structures of the apo-tetramer and the product bound octamer are a physiological phenomenon, or are a result of crystallization, the oligomeric state of *Mtb* FolB in solution was determined by analytical ultracentrifugation. At low concentrations of *Mtb* FolB (3 μM) in solution, sedimentation equilibrium ultracentrifugation of the protein alone gave a molecular mass of approximately $57.5(\pm 5)$ kDa (Figure 6(a)) which is within 5% of the predicted molecular mass of a tetramer (52.4 kDa). With the addition of 20 μM of substrate, 7,8-dihydroneopterin, the molecular mass of *Mtb* FolB increased considerably to approximately $96.3(\pm 10)$ kDa (Figure 6(b)) which is within 12% of the predicted molecular mass of an octamer (108.8 kDa). Further analysis of the apo-tetrameric data, gave a calculated association constant ($K_{a,\text{conc}}$) for the apo-tetramer/octamer equilibrium of $16,700(\pm 10,000) \text{ M}^{-1}$. The observed $K_{a,\text{conc}}$ indicates that at

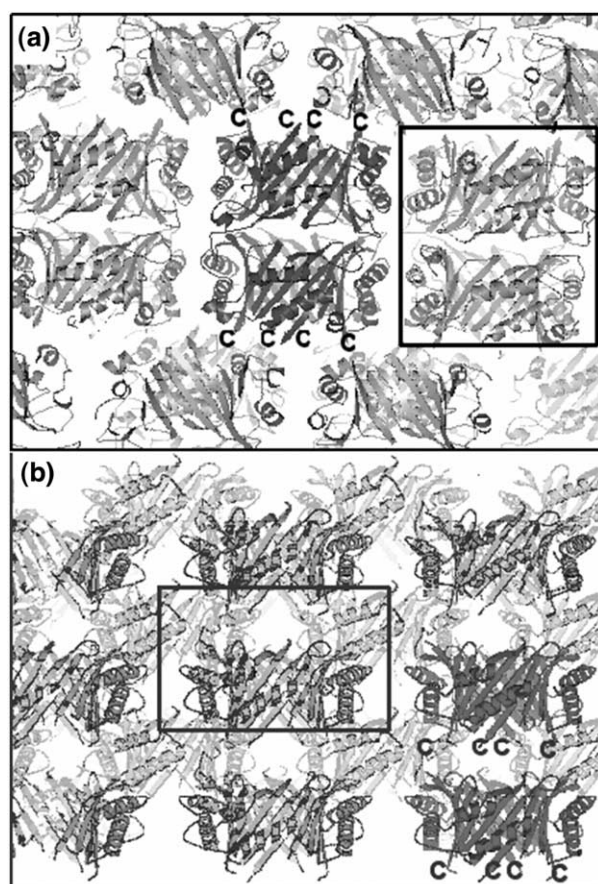


Figure 3. Illustration of the tetramer packing for *Mtb* FolB in the $P2_1$ and $I4$ forms which show there is an octamer in the $P2_1$ form and a certain tetramer in the $I4$ form. (a) In the *Mtb* FolB $P2_1$ form, there are eight molecules in the asymmetric unit and one of these octamers is high-lighted in dark grey. The unit cell is denoted by a black box. The octamers pack together in perfect planes as seen in the Figure. The C termini are labeled to illustrate head-to-head packing of the tetramers. (b) *Mtb* FolB $I4$ form has a monomer in its asymmetric unit. There are tetramers observed in the crystal packing as seen in the *Mtb* FolB $P2_1$ form. The tetramers pack together with no extensive contacts and therefore do not form an octamer as seen in the $P2_1$ form. Two tetramers are highlighted in dark grey to illustrate that there is no octamer in the *Mtb* FolB $I4$ form even though it is the same molecule. The unit cell is denoted by a black box. The C termini of the tetramers are labeled to illustrate the head-to-tail stacking. (a) and (b) were generated by PYMOL.

a concentration of $94(\pm 50)$ μM there is an equal ratio of both tetrameric and octameric forms in the absence of substrate. These results imply that *Mtb* FolB could be allosterically regulated as the oligomeric state of *Mtb* FolB changes in the presence of substrate.

Is *Mtb* FolB an allosterically regulated enzyme?

To verify that *Mtb* FolB is an allosterically

regulated enzyme we measured the activity of *Mtb* FolB at varying concentrations of 7,8-dihydro-pterin ($0.05\text{--}4$ μM) at room temperature. The relative initial reaction rates of *Mtb* FolB at varying concentrations of 7,8-dihydroneopterin showed sigmoidal kinetics and Hill plot analysis revealed a $K_{0.5}$ of $480(\pm 33)$ nM for 7,8-dihydroneopterin (Figure 7). Furthermore a Hill coefficient of $2.0(\pm 0.2)$ indicates that *Mtb* FolB exhibits positive cooperativity and has two types of substrate-binding sites: a low affinity site and a much higher affinity site.

Discussion

The observed apo-tetrameric form of *Mtb* FolB appears unique among FolB holoproteins

FolB holoproteins isolated from numerous sources appear to be octameric in the absence of substrate, suggesting that the observed apo-tetrameric state of *Mtb* FolB is unique among FolB holoproteins to-date. The crystal structures of *S. aureus* FolB and *Arabidopsis thaliana* FolB show the enzymes in their octameric state with and without substrate.^{7,8} Similarly, sedimentation equilibrium analysis have shown that both *Escherichia coli* FolB and *Haemophilus influenzae* FolB also persist in their octameric forms in the absence of substrate.⁶ In contrast, two FolB-like domains of a multi-functional folate biosynthetic protein from the fungal pathogen *Pneumocystis carinii*, when expressed together demonstrate characteristics of an associating–dissociating equilibrium. It was further shown that the enzyme was functional as an octamer.⁹

The comparison of the octameric structures of *Mtb* FolB and *S. aureus* FolB

Comparison of the *S. aureus* and *A. thaliana* FolB structures to the octameric state of *Mtb* FolB show distinct differences in assembly which may account for the fact that the stability of the *Mtb* FolB octamer appears to be much more sensitive to ligand binding. This increased sensitivity in the *Mtb* enzyme can be explained by structural differences between the *Mtb* and *S. aureus* enzymes especially at the tetramer–tetramer interface and in the pterin-binding pocket.⁷ The interactions within the FolB structures of *S. aureus* and *A. thaliana* are nearly identical,^{7,8} and therefore our comparison will focus on the *S. aureus* FolB structure.

The binding of product in the *Mtb* FolB octameric structure appears to have a more complex hydrogen-bonding network than that of the *S. aureus* FolB octameric structure. In both *Mtb* and *S. aureus* FolB models, there are conserved interactions between three conserved residues Tyr54B, Leu72A and Glu74A (Figure 2(a)) and the pterin ring⁷ (A and B represent the monomers at the interface of an active site). Additionally, in the *Mtb*

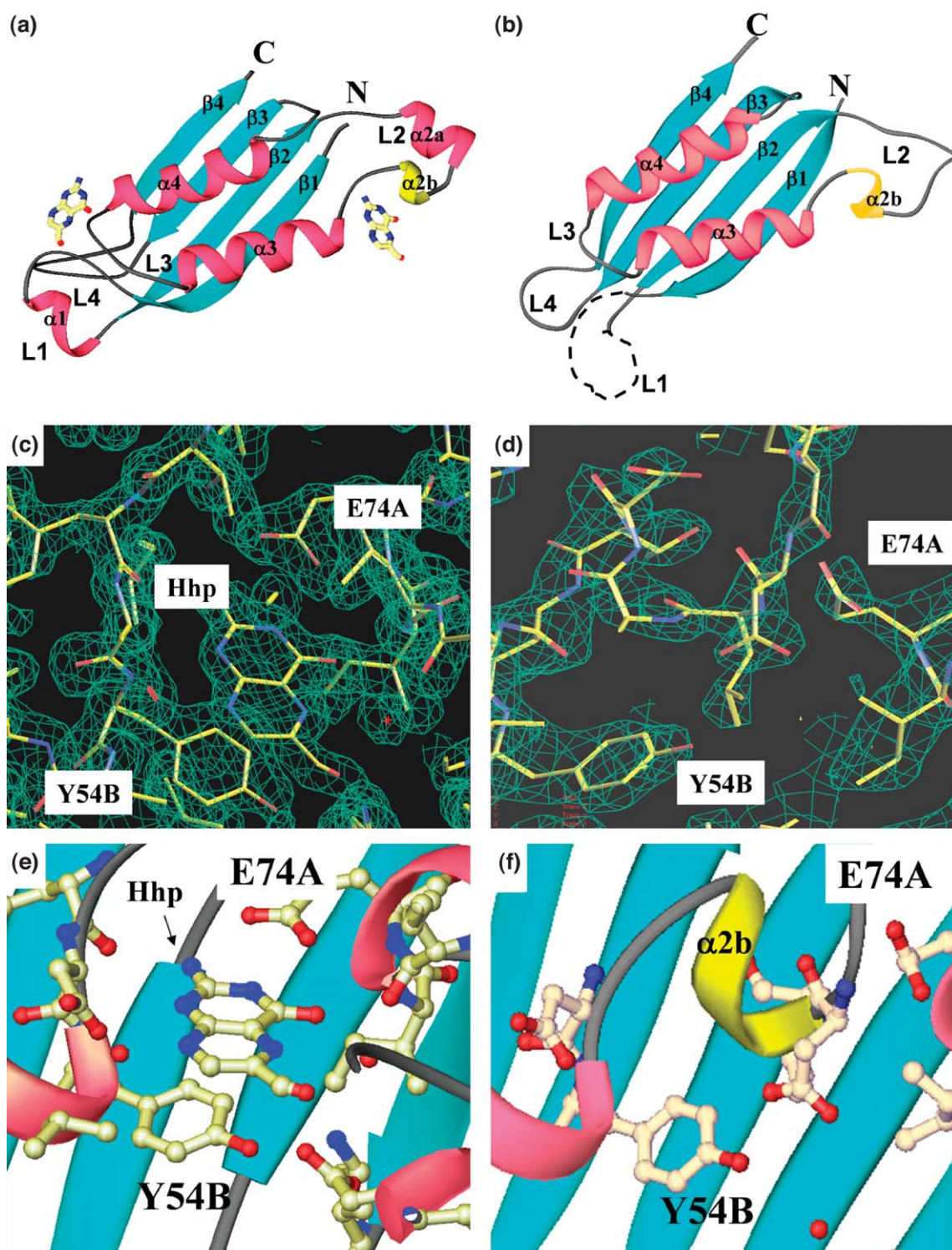


Figure 4. Monomers and active sites of *Mtb* *FolB* in the $P2_1$ and $I4$ forms. (a) and (b) The ribbon diagrams of the *Mtb* *FolB* monomers from the $P2_1$ octamer and the $I4$ tetramer forms, respectively. Comparing the ribbon diagrams in (a) and (b), the major differences in the two monomers is that loop L1 is disordered, $\alpha 2a$ -helix is no longer ordered, 3_{10} -helix ($\alpha 2b$) has shifted its position, and loops L2 and L4 have shifted their positions in the tetrameric $I4$ form (b) compared to the $P2_1$ octameric form (a). (c) and (d) A view of the composite omit $2F_o - F_c$ electron density maps at the active site of the *Mtb* *FolB* $P2_1$ and $I4$ forms, respectively. The electron density is contoured at 1.2σ . Try54B and Glu74A are labeled in the active sites. A and B represent the monomers at the interface of an active site. The major difference between the two active sites is that 6-hydroxymethyl-7,8-dihydropterin (Hhp) is modeled into the structure of the *Mtb* *FolB* octameric $P2_1$ form (c), whereas there is no electron density of the product in the *Mtb* *FolB* tetrameric $I4$ form (d). In fact, there appears to be electron density for residues in the proposed active site cavity of the *Mtb* *FolB* tetrameric $I4$ form. This is illustrated more clearly in a ribbon diagram of the active sites of the *Mtb* *FolB* $P2_1$ and $I4$ forms, (e) and (f), respectively. The 6-hydroxymethyl-7,8-dihydropterin is denoted by Hhp in (e). In the *Mtb* *FolB* tetrameric $I4$ form, the

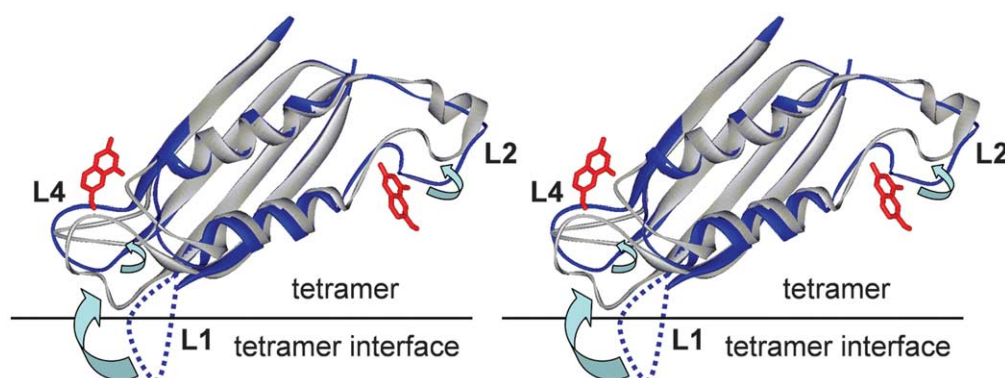


Figure 5. Superpositioning of the *Mtb* FolB monomers of the apo-tetrameric and octameric forms by three-dimensional structural alignments. Shown in a stereo view are the C α traces for *Mtb* FolB octameric form (blue, thick line) and *Mtb* FolB apo-tetrameric (grey, thin line) with the disordered loop L1 depicted by a thick blue broken line. Also, shown are the two product molecules in red, modeled in from the octameric structure of *Mtb* FolB. One can see the conformation changes in loops L1, L2 and L4 upon addition of substrate and the proposed movement is indicated with light blue arrows. The three-dimensional structural alignment was carried out with ALIGN.²⁴

FolB active site, the N⁸ atom of 6-hydroxymethyl-7,8-dihydropterin is hydrogen-bonded to O ^{ϵ 1} of Asp53B and the hydroxyl group is hydrogen-bonded to both the main-chain amide of Val18A and the ϵ -amino group of Lys99A.

In the *S. aureus* FolB structure, tetramer–tetramer stability is mainly achieved through hydrophobic interactions, whereas in the *Mtb* FolB octameric structure this interface is mainly stabilized through ion-pairing. The hydrophobic interactions of the *S. aureus* FolB structure are between the side-chains of the residues in loops L1 and L4 as well as a symmetry-related parallel stacking of His108 imidazole rings between tetramers.⁷ In the *Mtb* FolB octameric structure, there are four weak ion-pairs per monomer between residue side-chains and the backbone carbonyls which are less than 5.0 Å apart, Arg28A:Phe108E, His21A:His21E, Gln101A:Gln101E and His13A:Pro105E, where residues are also located in loops L1 and L4 (where A represents a monomer in one tetramer and E represents the interacting monomer in the other tetramer). There is also one hydrophobic interaction between Pro103A and Ala25E. Perhaps tetramer–tetramer interface ion-pair interactions found in *Mtb* FolB permit allosteric regulation in contrast to the hydrophobic interactions seen in *S. aureus* FolB.

***Mtb* FolB tetramer–octamer equilibrium**

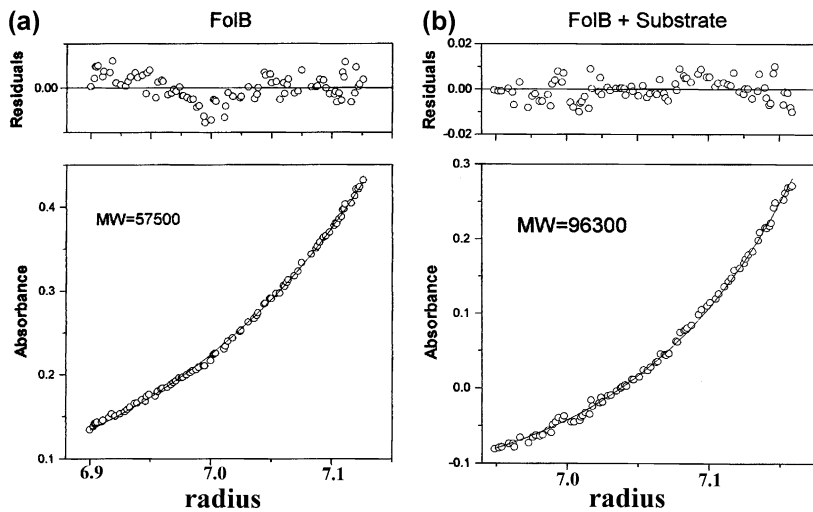
In the *Mtb* FolB apo-tetrameric form the active-site catalytic machinery is not fully formed, as helix α 2b is in the vicinity of the active site and loop L1 which contains the catalytic residue Glu22 is disordered. When substrate binds at the interface

between two monomers in the tetrameric ring, the active site must be fully formed. For this to occur, catalytic and substrate-binding residues must reposition themselves, and loop L2 must be displaced from within the active site (Figure 5). The main residues which shift on substrate binding are Try54B (α -helix 3B), Leu72A and Glu74A (both in the vicinity of loop L3A), and the proposed catalytic residues Glu22A (loop L1A) and Lys99A (loop L4A).^{7,8} These subtle conformational changes at the interface between two monomers upon substrate binding, provides the correct tetrameric interface for the active *Mtb* FolB octameric state to form.

Our results suggest that *Mtb* FolB is inactive in its apo-tetrameric form and upon substrate binding, the active octameric state of *Mtb* FolB forms, implying that *Mtb* FolB is allosterically regulated through oligomerization. Both hemoglobin¹⁰ and ribulose-5-phosphate 3-epimerase¹¹ offer examples of oligomers that display positive cooperative behavior. In the case of ribulose-5-phosphate 3-epimerase, the affinity of the disassembled subunit for ligand is decreased,¹¹ as is observed for *Mtb* FolB, whereas in the case of hemoglobin the opposite effect is observed where the affinity of the disassembled subunit for oxygen increases.¹⁰

Based on the structural and biochemical information presented here, two simple models of allosteric regulation for *Mtb* FolB are described below (one should note that there are many more complicated models for regulation). From the Hill plot analysis (Figure 7), it is assumed that there are two types of substrate-binding sites, a low affinity site and a high affinity site for *Mtb* FolB. The first model is that substrate binding drives the formation of the fully active *Mtb* FolB octamer (Figure 8(a)).

3_{10} -helix (colored in yellow) is positioned within the active site, possibly preventing binding of substrate. Try54B and Glu74A are labeled in the active sites. In the ribbon diagrams α -helices, the 3_{10} -helix, β -strands and random coil are shown in pink, yellow, cyan and grey, respectively. The atoms of the residues are colored as follows: carbon, nitrogen and oxygen are off-white, blue and red, respectively.



mental data (circles) with a single exponential (continuous line), and include roughly 2–3% (residuals are in top panels). The molecular weight of *Mtb* FolB without substrate suggests at this concentration it exists as a tetramer in solution, whereas the molecular weight of *Mtb* FolB with substrate suggests it exists as a 7-mer to an octamer in solution.

One may postulate that upon binding the substrate in the low affinity sites of the inactive tetrameric state, octamer formation would be induced and generate high affinity sites in the octameric complex. The second model is that oligomerization is required before substrate binding (Figure 8(b)). One may postulate that formation of the octamer is *Mtb* FolB concentration dependent. Thus, when *Mtb* FolB apo-tetrameric state reaches a critical concentration, an apo-octameric state will form, allowing for substrate binding where there are both low and high affinity substrate-binding sites. This model appears less probable as the association constant ($94(\pm 50) \mu\text{M}$) calculated for apo-tetramer to form apo-octamer is considerably higher than the expected physiological concentration of the protein within a cell. Hence, the substrate-driven oligomerization model for allosteric regulation of *Mtb* FolB is

favoured over the oligomerization-first-driven model.

Why would *Mtb* FolB be allosterically regulated in *M. tuberculosis*?

We hypothesize that *Mtb* FolB is allosterically regulated as a mechanism for protection against oxidative damage as its host produces hydrogen peroxide as a defense mechanism against pathogenic bacteria. The substrate of *Mtb* FolB, 7,8-dihydroneopterin, is a bifunctional molecule as it can function as both a potent antioxidant and a substrate for *Mtb* FolB. Recent studies have shown that in mammalian macrophage cells, intracellular mammalian 7,8-dihydroneopterin protect macrophage proteins against reactive oxygen species during inflammation.^{12,13} In these studies, it has

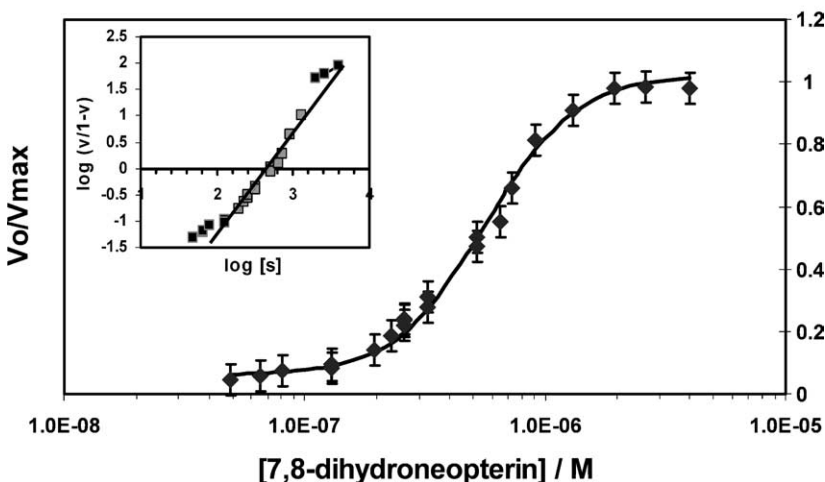


Figure 7. Kinetic analysis of *Mtb* FolB with substrate. *In vitro* activity of *Mtb* FolB (20 nM) with varying concentrations of substrate, 7,8-dihydroneopterin (ranging from 0.05 μM to 4 μM) in 50 mM Tris-HCl (pH 8.0) and 150 mM NaCl. The relative initial reaction rates of *Mtb* FolB at varying concentrations of 7,8-dihydroneopterin showed sigmoidal kinetics. The insert represents the corresponding Hill plot. Hill plot analysis revealed a $K_{0.5}$ of $480(\pm 33)$ nM for 7,8-dihydroneopterin and a Hill coefficient of $2.0(\pm 0.2)$ which indicates that *Mtb* FolB exhibits positive cooperativity and that there are two types of binding sites: a low affinity site and a much higher affinity site.

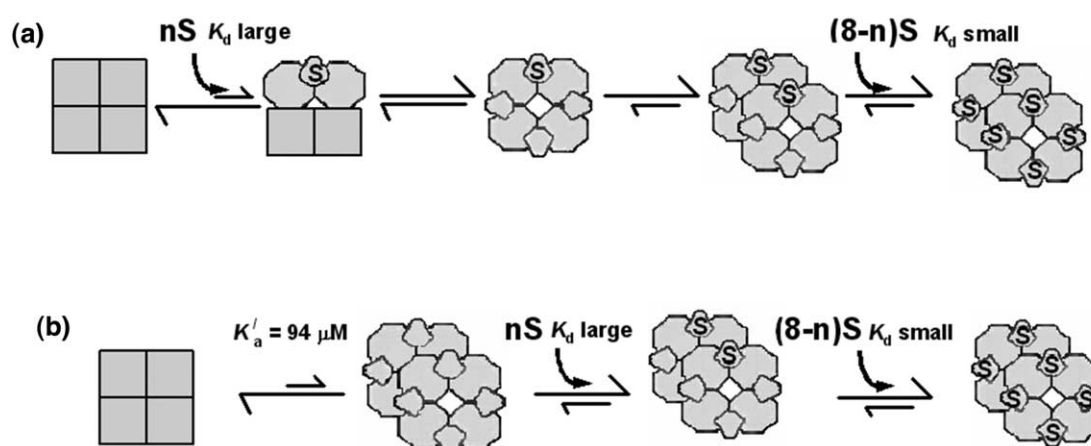


Figure 8. Two models for allosteric regulation of *Mtb* FolB. The squares represent the conformation of *Mtb* FolB monomer in the apo-tetrameric state with its partially formed active site. The conformation of a monomer from the octameric state is represented by an octagon with an active site between monomers. In both panels, “ K_d large” represents the low affinity substrate-binding sites, “ K_d small” represents the high affinity substrate-binding sites, “ n ” is equal to the number of substrate molecules bound to the lower affinity-binding site and “ K_a' ” is the association constant between apo-tetramer to apo-octamer. (a) Substrate-driven oligomerization allosteric mechanism. The mechanism is initiated by the binding of n substrate molecules in the low affinity binding sites of the tetramer state. This conformational change induces movement in the other monomers, promoting a tetramer which now has all monomers in the conformational state required to form the octamer. In the final step, upon octamer formation, the enzyme may bind its remaining substrate molecules in the high affinity binding sites. (b) Oligomerization-first-driven allosteric mechanism. Concentration of the apo-tetrameric state is such that the apo-octameric state forms. The octamer will first bind n substrate molecules to its low affinity binding sites and then the remaining substrate molecules to its high affinity binding sites, resulting in a fully active enzyme.

also been shown that 7,8-dihydroneopterin acts as an antioxidant by inhibiting low density lipoprotein oxidation, peroxyl radical formation and superoxide generation.^{12,13} Perhaps *M. tuberculosis* may also utilize 7,8-dihydroneopterin in a similar manner. In fact, when *M. tuberculosis* resides in an oxidative environment such as macrophages or granulomas, 7,8-dihydroneopterin could protect *M. tuberculosis* against oxidative damage. Thus, if the host exerts oxidative stress upon the bacterium and 7,8-dihydroneopterin acts as an antioxidant in *M. tuberculosis*, then 7,8-dihydroneopterin will not reach the concentration required to form the active octameric FolB state. However, when oxidative stress diminishes, the concentration of 7,8-dihydroneopterin would increase to the critical level to overcome the initially low substrate-binding affinity to form the active, octameric *Mtb* FolB state and the mycobacterium would continue with its normal folate biosynthetic pathway. To further reinforce this hypothesis, it has been shown that FolP the first committed step in the folate biosynthetic pathway which produces 7,8-dihydroneopterin, is up-regulated in granulomas which have an oxidative environment as compared to *in vitro* cultures (H. Rachman *et al.*, unpublished results).

Overall Conclusion

We have shown that a FolB homolog is an allosterically regulated enzyme, having an apo-tetrameric state not previously observed in FolB

holoproteins. We hypothesize that the instability of the tetramer–tetramer interface of *Mtb* FolB is a result of differences between the interactions at the tetramer–tetramer interface and in ligand binding which are necessary for regulating the *Mtb* FolB enzyme, as compared to other structures of FolB homologs. We also presented two simple models of allosteric regulation of which the substrate-driven oligomerization model is favored, together with a hypothesis for allosteric regulation unique to *Mtb* FolB. Further kinetic studies are necessary to completely unravel the complicated scenario of *Mtb* FolB allosteric regulation. Our results suggest that *Mtb* FolB may be a viable target for rational drug development against tuberculosis.

Materials and Methods

Materials

The DNA QIAprep Spin miniprep kit and QIAquick gel extraction kit were purchased from Qiagen. Restriction enzymes and T4 DNA ligase were purchased from New England Biolabs. HiTrap chelating (1 ml and 5 ml) and size exclusion columns were purchased from Amersham Pharmacia. We purchased Advantage-GC genomic PCR polymerase from Clontech, and biotinylated thrombin and pET22b+ vector from Novagen. *M. tuberculosis* genomic DNA, strain H37Rv, is a generous gift from Dr John T. Belisle at Colorado State University. All primers were synthesized by GibcoBRL.

Cloning of *Mtb* FolB

The gene that encodes for *Mtb* FolB is annotated as Rv3607c. The 5' primer starts with the NdeI restriction site which includes the start-codon and the first 30 nucleotides of Rv3607c. The 3' primer ends with a HindIII restriction site which precedes an engineered thrombin cleavage site which encodes for the amino acid residues GVPRG, and then the final 20 nucleotides of the gene, Rv3607c, not including the stop-codon. The PCR reaction was carried out using Advantage-GC genomic PCR polymerase. The resulting product was excised from a 2% (w/v) agarose gel and purified using the gel extraction kit. The PCR product was ligated into a linearized blunt vector, pCR-BluntII-TOPO (Invitrogen), and then transformed into OneShot TOP10 *E. coli* cells (Invitrogen). The gene was then double-digested from the blunt vector with NdeI and HindIII, and the plasmid pET22b+ was also digested with the same restriction enzymes. The cut gene was then ligated into the cut pET22b+ vector and transformed into *E. coli* BL21 (DE3) cells (Novagen). The presence of the correct gene and thrombin cleavage site was confirmed by sequencing using T7 promoter and reverse primers (Davis sequencing, Davis, CA).

Overexpression and purification of *Mtb* FolB

Mtb FolB was purified from the pET22b+ plasmid containing Rv3607c gene using BL21 (DE3) cells. Cells were grown aerobically at 37 °C in LB medium containing ampicillin (100 µg/ml). Protein expression was induced by addition of 1 mM isopropyl-beta-D-thiogalactoside at an A_{600} of ~1.0 and the cells were harvested four hours after induction. *Mtb* FolB was expressed in the soluble fraction at a level of approximately 10 mg/l of cells. Cell harvesting, disruption and protein purification utilized the same protocols as described for Rv1926c (MPT63).¹⁴

Cleavage of *Mtb* FolB carbonyl-terminal His₆-tagged fusion with thrombin

To 20 mg of *Mtb* FolB-His₆-tag in thrombin cleavage buffer, 50 units of biotinylated thrombin was added and incubated overnight at 37 °C. To remove biotinylated thrombin, streptavidin-agarose was added (2 ml) and left for ten minutes before spinning the agarose down at 5000 rpm for five minutes. The cleaved protein was loaded over a Ni²⁺-charged HiTrap column (1 ml), the flow-through fractions which contained the cleaved protein were collected. The cleavage of the His₆-tag from *Mtb* FolB was verified on a SDS-PAGE gel and pure fractions were concentrated and then dialyzed against 50 mM Tris-HCl (pH 7.4), and 350 mM NaCl.

Crystallization, data collection, structure determination and refinement

Mtb FolB crystallized in two different space groups, *I4* and *P2*₁, which were solved and are presented here. For crystallization, *Mtb* FolB was 12 mg/ml in 350 mM NaCl and 50 mM Tris-HCl (pH 7.4). Crystals were grown by hanging drop-vapor diffusion against a reservoir and the drop size was 2 µl of protein and 2 µl of reservoir buffer. For space group *I4*, the reservoir condition was 1000 µl of 15% (w/v) PEG 4000 and 0.2 M sodium acetate (pH 7.6). The crystals were swiped through 1:1 reservoir condition and 50% (v/v) glycerol, and diffraction data was collected at 100 K. For space group *P2*₁, the reservoir

condition was 1000 µl of 11% PEG 4000, 0.1 M LiSO₄ and 0.1 M sodium acetate (pH 4.6). As before, the crystals were swiped through a 1:1 mixture of reservoir solution and 50% glycerol, and diffraction data was collected at 100 K. For *P2*₁ substrate-soaked crystals, 1 µl of 5 mM 7,8-dihydroneopterin was added to crystals in a 4 µl drop. *Mtb* FolB *I4* and *P2*₁ datasets were collected at BNL beamline X8C on an ADSC Quantum-4 charge-coupled device (CCD) and the substrate-soaked *P2*₁ FolB dataset was collected in-house on Raxis4+. All crystals were mounted in a cryogenic nitrogen stream at 700 K for data collection. Complete data sets were collected from single crystals. After autoindexing, images were indexed, integrated, reduced and scaled using DENZO and SCALEPACK.¹⁵ Data collection statistics are presented in Table 1.

Crystals in space group *P2*₁ contained eight monomers per asymmetric unit. The initial phases for the *P2*₁ *Mtb* FolB structure were determined by the stochastic evolutionary programmed molecular replacement method (EPMR).¹⁶ The search model was a poly-alanine octameric model of *S. aureus* FolB.⁷ The EPMR solution was used for automated model building was carried out by ARP/wARP in the "molrep" mode for all but three residues of each chain of the octamer.¹⁷ Refinement was subsequently carried out in CNS¹⁸ initially using NCS restraints. When the R_{work} reached 24%, the NCS constraints were released and the model was refined over the entire octamer. Model building was done in O.¹⁹ Electron-density for the product of FolB, 6-hydroxymethyl-7,8-dihydropterin, was observed in the *P2*₁ *Mtb* FolB structure, and one molecule of product was modeled per monomer. At this point the R_{work} and R_{free} were 20.2 and 24.4, respectively, at a resolution of 2.0 Å. Resolution of this model was then extended to 1.6 Å with the dataset soaked with substrate, 7,8-dihydroneopterin. Further refinement was done in CNS and then the final rounds of refinement and addition of water molecules were carried out in SHELXL†. The final structure was complete from Ala2 to Arg119 in each chain, with one product molecule per monomer. Due to lack of electron density for the side-chain of Try19C, it was modeled as alanine and so were Asp20B, Asp20C and Asp20D (the letters denote the amino acid chain). Six arginine residues had two distinct conformations which were also allowed for in the refinement, Arg23A, Arg23B, Arg15C, Arg15E, Arg23E, and Arg23F. The final data and refinement statistics are shown in Table 1 with the R_{work} and R_{free} values of 16.5 and 25.8, respectively. The stereochemistry and geometry of each *Mtb* FolB monomer was validated with PROCHECK²⁰ and ERRAT,²¹ and was found to be acceptable (e.g. no residues in the disallowed region of ϕ, ψ , space for *Mtb* FolB-product *P2*₁ model).

Crystals in space group *I4* contained one monomer per asymmetric unit. The *I4* *Mtb* FolB structure was also determined by EPMR using a search model of the monomer from the *P2*₁ *Mtb* FolB structure. The EPMR solution was used for initial refinement in CNS. After several rounds of refinement, the R_{work} was no longer improving at around 35%. At this point all the loop regions were removed, residues 14–26 (L1), 37–52 (L2), 69–78 (L3) and 98–110 (L4), and a further round of refinement was performed, which allowed rebuilding of all the residues removed except loop L1 containing residues 15–25 which had no apparent electron density. Four residues were modeled as alanine residues due to lack of side-chain electron density, Arg70, Lys71, Leu72

† <http://shelx.uni-ac.gwdg.de/SHELX/>

and Lys99. Further refinement cycles and the addition of water and acetate molecules resulted in a satisfactory R_{work} and R_{free} values of 17.9 and 23.4, respectively. The stereochemistry and geometry of the residues of the monomer of 14 *Mtb* FolB were validated with both PROCHECK²⁰ and ERRAT.²¹ One residue was found in the disallowed region of ϕ, ψ space (Pro69), though this residue fits the observed electron density well.

Isolation of the tetrameric state of FolB

Mtb FolB was further purified on a gel filtration column (HiLoad 16/60 Superdex 75 prep grade column) to strip any bound product, 6-hydroxymethyl-7,8-dihydropterin for analytical centrifugation experiments. The protein and product were eluted with 50 mM Tris-HCl (pH 7.4) and 350 mM NaCl at a flow-rate of 0.5 ml/min. *Mtb* FolB had a retention time of 1:05 hour and the pterin had a retention time of 1:54 hour.

Analytical ultracentrifugation

Sedimentation equilibrium was performed with *Mtb* FolB concentrations of 3 μM with the addition of 20 μM substrate, 7,8-dihydroneopterin, at 20 °C. All samples were buffered in 350 mM NaCl and 50 mM Tris-HCl (pH 7.4). Protein concentration was monitored by absorption at 228 nm and 280 nm. Sedimentation equilibrium profiles were measured at 10,500 rpm, experiments and calculations were carried out as described.²²

To determine the association constant (K_a) for tetrameric to octameric form, an equilibrium sedimentation experiment was carried out with three different concentrations of tetrameric-14 FolB protein (50 μM , 30 μM and 10 μM) at two different rotor speeds (8000 rpm and 10,500 rpm). The K_a was calculated using the Beckman Origin-based software (Version 3.01). The calculated K_a is in absorbance units and assumes that the tetramer is a monomer and the octamer is a dimer. To convert the K_a to units of concentration, equation (1) was utilized, where $K_{a,\text{abs}}$ is the K_a with absorbance units, $K_{a,\text{conc}}$ is the K_a with molarity units, ϵ is the extinction coefficient for the tetramer and l is the pathlength of the cell:

$$K_{a,\text{conc}} = K_{a,\text{abs}} \epsilon l / 2 \quad (1)$$

Assay for 7,8-dihydroneopterin aldolase activity

The initial rate of reaction of *Mtb* FolB was quantified using a fluorescence-based kinetic enzyme assay monitoring formation of the reaction product 6-hydroxymethyl-7,8-dihydropterin as described.²³

Protein database accession codes

The coordinates and structure factors for the crystal structures of octameric *Mtb* FolB complexed with product and the monomer of apo-tetrameric *Mtb* FolB were deposited with the Protein Data Bank (RCSB)[†] as entry 1NBU and 1Z9W, respectively.

[†] <http://www.rcsb.org/pdb>

Acknowledgements

This work has been supported by grants from the National Institutes of Health, DOE and HHMI (for D.E.) The authors thank Dr John T. Belisle, Colorado State University and NIH, NIAID Contract NO1 AI-75320 for the generous supply of *M. tuberculosis* H37Rv genomic DNA. We thank Dr Duilio Cascio for invaluable help with data collection and general crystallography. We also thank Brookhaven National Laboratory for the use of beamline X8C of the National Synchrotron Light Source in particularly Joel Berendzen, Li Wei Hung and Leonid Flaks. Also, special thanks to Tom Terwilliger at Los Alamos National Laboratories and the anonymous referee for helpful comments.

References

1. The World Health Organization (1998). The World Health Report 1998: Life in the 21st Century—A Vision for All, Geneva, Switzerland.
2. Goulding, C. W., Apostol, M., Anderson, D. H., Gill, H. S., Smith, C. V., Kuo, M. R. *et al.* (2002). The TB structural genomics consortium: providing a structural foundation for drug discovery. *Curr. Drug Targets Infect. Disord.* **2**, 121–141.
3. Maden, B. E. (2000). Tetrahydrofolate and tetrahydromethanopterin compared: functionally distinct carriers in C1 metabolism. *Biochem. J.* **350**, 609–629.
4. Achari, A., Somers, D. O., Champness, J. N., Bryant, P. K., Rosemond, J. & Stammers, D. K. (1997). Crystal structure of the anti-bacterial sulfonamide drug target dihydropteroate synthase. *Nature Struct. Biol.* **4**, 490–497.
5. Fleischmann, R. D., Adams, M. D., White, O., Clayton, R. A., Kirkness, E. F., Kerlavage, A. R. *et al.* (1995). Whole-genome random sequencing and assembly of *Haemophilus influenzae* Rd. *Science*, **269**, 496–512.
6. Haussmann, C., Rohdich, F., Schmidt, E., Bacher, A. & Richter, G. (1998). Biosynthesis of pteridines in *Escherichia coli*. Structural and mechanistic similarity of dihydroneopterin-triphosphate epimerase and dihydroneopterin aldolase. *J. Biol. Chem.* **273**, 17418–17424.
7. Hennig, M., D'Arcy, A., Hampele, I. C., Page, M. G., Oefner, C. & Dale, G. E. (1998). Crystal structure and reaction mechanism of 7,8-dihydroneopterin aldolase from *Staphylococcus aureus*. *Nature Struct. Biol.* **5**, 357–362.
8. Bauer, S., Schott, A. K., Illarionova, V., Bacher, A., Huber, R. & Fischer, M. (2004). Biosynthesis of tetrahydrofolate in plants: crystal structure of 7,8-dihydroneopterin aldolase from *Arabidopsis thaliana* reveals a novel adolase class. *J. Mol. Biol.* **339**, 967–979.
9. Thomas, M. C., Ballantine, S. P., Bethell, S. S., Bains, S., Kellam, P. & Delves, C. J. (1998). Single amino acid substitutions disrupt tetramer formation in the dihydroneopterin aldolase enzyme of *Pneumocystis carinii*. *Biochemistry*, **37**, 11629–11636.
10. Mills, F. C., Johnson, M. L. & Ackers, G. K. (1976). Oxygenation-linked subunit interactions in human hemoglobin: experimental studies on the concentration dependence of oxygenation curves. *Biochemistry*, **15**, 5350–5362.
11. Karmali, A., Drake, A. F. & Spencer, N. (1983).

- Purification, properties and assay of D-ribulose 5-phosphate 3-epimerase from human erythrocytes. *Biochem. J.* **211**, 617–623.
12. Duggan, S., Rait, C., Platt, A. & Gieseg, S. (2002). Protein and thiol oxidation in cells exposed to peroxyl radicals is inhibited by the macrophage synthesised pterin 7,8-dihydroneopterin. *Biochim. Biophys. Acta*, **1591**, 139–145.
 13. Wirleitner, B., Obermoser, G., Bock, G., Neurauter, G., Schennach, H., Sepp, N. & Fuchs, D. (2003). Induction of apoptosis in human blood T cells by 7,8-dihydroneopterin: the difference between healthy controls and patients with systemic lupus erythematosus. *Clin. Immunol.* **107**, 152–159.
 14. Goulding, C. W., Parseghian, A., Sawaya, M. R., Cascio, D., Apostol, M. I., Gennaro, M. L. & Eisenberg, D. (2002). Crystal structure of a major secreted protein of *Mycobacterium tuberculosis*-MPT63 at 1.5-Å resolution. *Protein Sci.* **11**, 2887–2893.
 15. Otwinowski, Z. & Minor, W. (1996). Processing of X-ray diffraction data collected in oscillation mode. In *Methods in Enzymology* (Carter, C. W. & Sweet, R. M., eds), vol. 276, Academic Press, New York.
 16. Kissinger, C. R., Gehlhaar, D. K., Smith, B. A. & Bouzida, D. (2001). Molecular replacement by evolutionary search. *Acta. Crystallog. sect. D: Biol. Crystallog.* **57**, 1474–1479.
 17. Perrakis, A., Morris, R. & Lamzin, V. S. (1999). Automated protein model building combined with iterative structure refinement. *Nature Struct. Biol.* **6**, 458–463.
 18. Brunger, A. T., Adams, P. D., Clore, G. M., DeLano, W. L., Gros, P., Grosse-Kunstleve, R. W. *et al.* (1998). Crystallography & NMR system: a new software suite for macromolecular structure determination. *Acta. Crystallog. sect. D: Biol. Crystallog.* **54**, 905–921.
 19. Jones, T. A., Zou, J. Y., Cowan, S. W. & Kjeldgaard, M. (1991). Improved methods for building protein models in electron density maps and the location of errors in these models. *Acta. Crystallog. sect. A*, **47**, 110–119.
 20. Laskowski, R. A., Moss, D. S. & Thornton, J. M. (1993). Main-chain bond lengths and bond angles in protein structures. *J. Mol. Biol.* **231**, 1049–1067.
 21. Colovos, C. & Yeates, T. O. (1993). Verification of protein structures: patterns of nonbonded atomic interactions. *Protein Sci.* **2**, 1511–1519.
 22. Mura, C., Kozhukhovskiy, A., Gingery, M., Phillips, M. & Eisenberg, D. (2003). The oligomerization and ligand-binding properties of Sm-like archaeal proteins (SmAPs). *Protein Sci.* **12**, 832–847.
 23. Sanders, W. J., Nienaber, V. L., Lerner, C. G., McCall, J. O., Merrick, S. M., Swanson, S. J. *et al.* (2004). Discovery of potent inhibitors of dihydroneopterin aldolase using CrystaLEAD high-throughput X-ray crystallographic screening and structure-directed lead optimization. *J. Med. Chem.* **47**, 1709–1718.
 24. Shindyalov, I. N. & Bourne, P. E. (1998). Protein structure alignment by incremental combinatorial extension (CE) of the optimal path. *Protein Eng.* **11**, 739–747.

Edited by I. Wilson

(Received 30 October 2004; received in revised form 25 February 2005; accepted 7 March 2005)